American Mineralogist, Volume 85, pages 1437–1446, 2000

Rare-earth elements in chlorapatite [$Ca_{10}(PO_4)_6Cl_2$]: Uptake, site preference, and degradation of monoclinic structure

MICHAEL E. FLEET,[1,*] XIAOYANG LIU,[1] AND YUANMING PAN[2]

[1]Department of Earth Sciences, University of Western Ontario, London, Ontario N6A 5B7, Canada
[2]Department of Geological Sciences, University of Saskatchewan, Saskatoon, Saskatchewan S7N 5E2, Canada

ABSTRACT

Differences in the inter- and intracrystalline partitioning behavior of rare earth elements (REE) between chlorapatite (ClAp), fluorapatite (FAp), and hydroxylapatite (OHAp) are directly or indirectly related to substitution mechanism and spatial accommodation. The substitution of REE for Ca is charge compensated by Na in ClAp, Na and Si in FAp, and Si in OHAp. Twinned crystals of REE-substituted ClAp [La-ClAp, Nd-ClAp, Sm-ClAp, Dy-ClAp; $Ca_{10-2y}Na_yREE_y(PO_4)_6Cl_2$, with $y = 0.05$–0.09; space group $P2_1/b$] have been grown from SiO_2-bearing, H_2O- and Na-rich phosphate-chloride melts, and their hexagonal ($P6_3/m$) subcell structures refined at room temperature with single-crystal X-ray intensities to $R = 0.020$–0.023. The crystal/melt partition coefficients for La, Nd, Sm, and Dy are 0.073, 0.128, 0.122, and 0.101. Thus, uptake of REE is up to two orders of magnitude lower in ClAp than in REE-substituted FAp and OHAp crystallized under equivalent conditions, but remains peaked at Nd. REE site occupancy ratios [(REE-Ca2)/(REE-Ca1)] obtained from direct refinement of electron densities are 0.71, 1.11, 0.21, and 0.09 for La-, Nd-, Sm-, and Dy-ClAp, respectively, and are consistent with relative change in Ca-O bond distances and sizes of Ca polyhedra. Thus, La, Sm, and Dy favor the Ca1 position of ClAp, not Ca2, as in FAp and OHAp; this unusual site preference is attributed to the large increase in size (6–8%) and distortion of the $Ca2O_6X$ polyhedron on substitution of Cl for (F,OH). The slight preference of Nd for Ca2 and the peaking of REE uptake at Nd are attributed to a 4*f* crystal-field contribution, which is revealed by an anomalous decrease in the Ca2-O1 bond length and volume of the $Ca2O_6X$ polyhedron in Nd-ClAp, Nd-Fap, and Nd-OHAp. The $P2_1/b$ structure of La-ClAp has been refined by detwinning the diffraction pattern, confirming that this monoclinic superstructure largely represents ordering of Cl atoms displaced along [001]. The $P2_1/b$ structure of Dy-OHAp has been refined similarly. The intensity of superstructure reflections decreases abruptly with increasing substitution of REE for Ca, showing that REE cations interfere with ordering of Cl atoms(and OH^- groups) during the $P6_3/m \rightarrow P2_1/b$ transition.

INTRODUCTION

Stoichiometric and near-stoichiometric chlorapatite [$Ca_{10}(PO_4)_6Cl_2$; ClAp] is monoclinic at room temperature with space group $P2_1/b$, $a = 9.642$ Å, $b = 19.273$ Å ($\approx 2a$), $c = 6.766$ Å, $\gamma = 120.02°$ (Mackie et al. 1972; Elliott 1994, 1998; Bauer and Klee 1993). The monoclinic structure is very similar to the hexagonal $P6_3/m$-type structure of apatite, but has an ordered arrangement of Cl atoms above and below $z = 1/4$ on the pseudohexagonal axis. Hexagonal ClAp is formed when either stoichiometric monoclinic ClAp is heated above about 350 °C (Bauer and Klee 1993) or Cl atoms are substituted by vacancies, F, or OH. When Cl is lost as $CaCl_2$, as little as 7% vacancies will break down the ordered continuity in the *c*-axis columns of Cl atoms (Prener 1971). Disordering of Cl atoms occurs when 0.32–0.72 atoms per formula unit (apfu) are substituted by F (Prener 1967) and 0.56–0.74 apfu by OH (Ruszala and Kostiner 1975). Chlorapatite loses $CaCl_2$ on heating to high temperature in air, particularly at temperatures close to the solidus. However, stoichiometric ClAp is readily synthesized from either a flux of molten $CaCl_2$, where $CaCl_2$ is present to excess (Prener 1967; Bauer and Klee 1993), or from hydrothermal solution, where the heating is confined in a vessel(Argiolas and Baumer 1978; Baumer et al. 1995). The hexagonal ($P6_3/m$) crystal structures of natural fluorapatite (FAp), hydroxylapatite (OHAp), and ClAp were compared in Hughes et al. (1989).

Rare earth elements (REE) substitute differentially for Ca in the apatite structure, with uptake being highest in the range Nd-Gd for natural apatite and near Nd for synthetic FAp (Fleet and Pan 1995, 1997a) and OHAp (Fleet et al. 2000), and being lowest for Lu (Fig. 1). The overall consistency of this behavior for rocks, melts, and solvents of widely different composition points to crystal-chemical control(s) on REE uptake. The two Ca positions (Ca1, Ca2) in the apatite structure offer quite different stereochemical environments. The nearest-neighbor environment of the Ca1 position (site symmetry 3) is a CaO_9 tricapped trigonal prism, which also can be regarded as 6 + 3 coordination. The environment of Ca2 (site symmetry *m*) is a CaO_6X irregular polyhedron formed by a hemisphere of 6 oxygen atoms capped by the volatile anion component (Fig. 2; see

* E-mail: mfleet@julian.uwo.ca

also figures in Hughes et al. 1989; Fleet and Pan 1995; Fleet et al. 2000). The strong preference of light REE for the Ca2 position in FAp and OHAp has been attributed variously to a control by substitution mechanism (Mackie and Young 1973; see also Gunawardane et al. 1982), electronegativity difference (Urusov and Khudolozhkin 1974), and equalization of bond valence (Hughes et al. 1991; Fleet and Pan 1995, 1997a, 1997b; Takahashi et al. 1998). Recently, Fleet et al. (2000) noted that the REE site occupancy ratio [(REE-Ca2)/(REE-Ca1)] in synthetic REE-FAp and REE-OHAp was proportional to the change in unit-cell volume, which pointed to some control by spatial accommodation of substituents in the apatite structure. Although these studies appeared to clarify the controls on site preference of REE in apatite, understanding of the crystal-chemical control(s) on REE uptake remained elusive. However, an anomalous structural change at Nd was revealed in a study of a series of binary-REE-substituted FAp (Fleet and Pan 1997a).

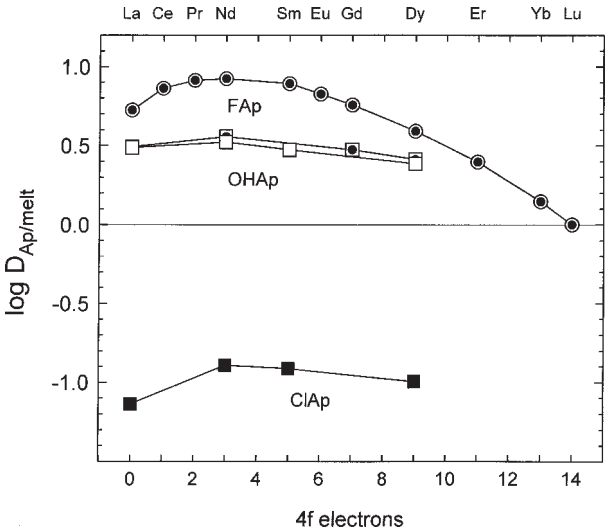

FIGURE 1. Melt-normalized REE contents of apatites synthesized from H_2O-bearing phosphate melts: REE-ClAp (present study; full squares); REE-FAp (Fleet and Pan 1995; open squares with dot; Fleet and Pan 1997b, minor contents of REE; open circles with dot); REE-OHAp (Fleet et al. 2000; open squares).

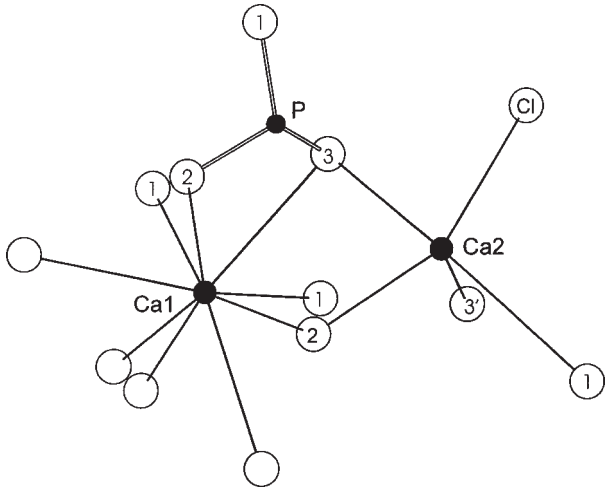

FIGURE 2. Nearest-neighbor environments of Ca1 and Ca2 in the $P6_3/m$ structure of La- chlorapatite (La-ClAp): *c*-axis projection; 1, 2, and 3 are oxygen atoms, and O3 and O3' are symmetry equivalent; Ca2-O3 = 2.549 Å (×2) and Ca2-O3' = 2.338 Å (×2; Table 4).

In previous studies (Fleet and Pan 1995, 1997a; Fleet et al. 2000), we have investigated REE uptake, REE site occupancy ratio, and structural change in several series of synthetic REE-substituted apatites: (1) La-FAp, Nd-FAp, Gd-FAp, Dy-FAp; $Ca_{10-6x-2y}Na_yREE_{6x+y}(P_{1-x}Si_xO_4)_6F_2$, with x = 0.04–0.05, y = 0.3–0.5; space group $P6_3/m$; (2) La,Gd-FAp, Ce,Dy-FAp, Pr,Er-FAp, Eu,Lu-FAp; with x = 0.02–0.03, y = 0.3–0.4; space group $P6_3/m$; and, (3) La-OHAp, Nd-OHAp, Sm-OHAp, Dy-OHAp; $Ca_{10-6x-2y}Na_yREE_{6x+y}(P_{1-x}Si_xO_4)_6(OH)_2$, with x = 0.036, y = 0.045; space group $P2_1/b$. This fourth study, on REE-substituted ClAp, arose from Fleet and Pan (1997b), who speculated that the volatile anion component (F, OH, Cl) might also be a significant factor in the selectivity of apatite for REE because of its marked influence on the stereochemical environment and effective size of the Ca2 site.

EXPERIMENTAL PROCEDURES

Single crystals of single-REE-substituted ClAp were grown from volatile-rich melts using a standard cold-seal hydrothermal reaction vessel, closely following procedures for REE-doped FAp and OHAp (Fleet and Pan 1995, 1997a; Fleet et al. 2000). Calcium REE silicate starting composition of stoichiometry $Ca_4REE_6(SiO_4)_6Cl_2$ was prepared from $CaCO_3$, REE_2O_3, SiO_2, and $CaCl_2$. Charges consisted of about 0.030 g of the starting composition, 0.01 g of NaCl, 0.030 g of a mixture of $CaCl_2 \cdot H_2O$ and P_2O_5 in the stoichiometric proportion of $Ca_{10}(PO_4)_6Cl_2$, and 0.01 g of deionized water contained in a sealed gold capsule 3.5 cm in length. Charges were heated initially to about 910 °C at 0.2 GPa, then cooled to 735 °C at 0.3 °C/min, maintained at 735 °C and 0.1–0.14 GPa for 13–39 h, and quenched in air and water. The products were digested in hot water, and washed several times in cold water. Crystals of ClAp were analyzed using a JEOL JXA-8600 electron microprobe (EPMA) at the University of Saskatchewan, operated at 15 kV, 10 nA with a beam diameter of 5 mm, and 30 s count times for Ca, P, and Cl, 60 s for Na and Si, and 90 s for REE. Standards included Durango FAp for Ca and P, jadeite for Na, quartz for Si, tugtupite for Cl, and synthetic REE phosphates for REE (Jarosewich and Boatner 1991). Two well-characterized apatite samples (Durango FAp and Bob Lake ClAp; Hunslow and Chao 1969) were used as secondary standards for monitoring the analysis of Cl. Each of the compositions reported in Table 1 represent averages of 10 individual spot analyses.

Single-crystal measurements were made at room temperature and pressure with a Nonius Kappa CCD diffractometer and graphite-monochromatized Mo$K\alpha$ X-radiation (50 kV, 32 mA, λ = 0.70926 Å). Reflection data were processed with the software packages DENZO and SCALEPACK (University of Texas Southwestern Medical Center at Dallas) and XDISPLAYF (University of Virginia Patent Foundation). SCALEPACK includes an empirical absorption correction based on equivalent reflection

intensities. Structure refinements were made with LINEX77 (State University of New York at Buffalo) and closely followed earlier procedures (Fleet and Pan 1995, 1997a; Fleet et al. 2000). Scattering factors for neutral atomic species and values of f' and f'' were taken, respectively, from Tables 2.2A and 2.3.1 of the *International Tables for X-ray Crystallography* (Ibers and Hamilton 1974). Experimental details are given in Table 2. Final parameters and selected bond distances and angles for the hexagonal $P6_3/m$ structures of La-, Nd-, Sm-, and Dy-ClAp are given in Tables 3 and 4, respectively, and observed and calculated structure factors in Table 5.[1]

All of the crystals investigated were mimetic twinned, with twin individuals related by 120% rotation about the *c* axis (pseudohexagonal axis; Mackie et al. 1972). The $P2_1/b$ structure of La-ClAp was refined using the Ca1 and Ca2 site occupancies from the $P6_3/m$ refinement, and correcting the observed structure factors of the subcell for the contribution from twinning after the procedure of Fleet and Burns (1990), assuming equal twin proportions (i.e., 0.3333; see below). Positional parameters are given in Table 6, and observed and calculated structure factors in Table 5; there were 4923 independent reflections, with 4119 having $I < 3\sigma_I$; $R = 0.027$, $R_w = 0.022$, and $s = 0.691$. We have also included in Tables 5 and 6 results of a similar refinement of the $P2_1/b$ structure of Dy-OHAp, the $P6_3/m$ struc-

[1]For a copy of Table 5, document item AM-00-054, contact the Business Office of the Mineralogical Society of America (see inside front cover of recent issue) for price information. Deposit items may also be available on the American Mineralogist web site (http://www.minsocam.org or current web address).

TABLE 1. Compositions of synthetic REE-bearing chlorapatite

Apatite	La-ClAp	Nd-ClAp	Sm-ClAp	Dy-ClAp
P_2O_5(wt%)	41.2(6)	39.8(5)	40.3(3)	40.2(6)
SiO_2	0.0	0.0	0.0	0.0
CaO	53.0(7)	50.9(6)	51.0(4)	51.6(4)
Na_2O	0.30(4)	0.51(8)	0.48(2)	0.42(7)
REE_2O_3	1.63(28)	2.89(44)	2.78(30)	2.42(40)
Cl	6.89(14)	6.65(11)	6.68(13)	6.69(17)
O≡Cl	1.55	1.50	1.51	1.51
Total	101.5	99.3	99.7	99.8
Chemical formulae based upon 16 cations*				
P	6.00	5.96	6.02	5.98
Si	0.00	0.00	0.00	0.00
Ca	9.79	9.68	9.65	9.74
Na	0.10	0.17	0.16	0.14
REE	0.10	0.18	0.17	0.14
Cl	2.00	1.99	1.99	1.99

* Ideal stoichiometry was assumed for X-ray structure refinement.

TABLE 2. Experimental details

	La-ClAp	Nd-ClAp	Sm-ClAp	Dy-ClAp
Experiment	AP156	AP127	AP158	AP159
Temperature* (°C)	735	735	735	735
Pressure* (GPa)	0.10	0.14	0.10	0.10
Time† (h)	13	39	13	13
Crystal size ($mm^3 \times 10^3$)	0.56	0.59	0.47	0.52
crystal shape	stubby prism	stubby prism	stubby prism	stubby prism
μ‡(cm^{-1})	32.33	34.28	34.62	35.01
a (Å) ($P6_3/m$)	9.6499(4)	9.6474(4)	9.6492(3)	9.6487(5)
c (Å)	6.7725(3)	6.7747(3)	6.7668(2)	6.7652(3)
Reflections-unique	841	952	1215	746
Reflections-number with ($I<3\sigma_{(I)}$)	574	677	788	508
Refined parameters	42	42	42	42
R	0.023	0.020	0.021	0.021
R_w§	0.020	0.020	0.018	0.017
s§	0.813	0.920	0.881	0.723
Extinction ($\times 10^4$)	0.0031(2)	0.0039(1)	0.0033(1)	0.0023(1)
Δρ|| ($eÅ^{-3}$) (+)	0.44	0.45	0.44	0.34
(–)	0.38	0.32	0.40	0.30
a (Å) ($P2_1/b$)	9.6501(4)	9.6475(5)	9.6493(3)	9.6486(5)
b	2a	2a	2a	2a
c (Å)	6.7724(3)	6.7747(3)	6.7668(2)	6.7652(3)
γ(°)	120	120	120	120

* Temperature and pressure of crystal synthesis; XRD measurements were made at room temperature and pressure.
† Time at final temperature.
‡ μ is linear absorption coefficient.
§ Least-squares refinement parameters: *R* is residual index; *Rw* is weighted residual index; s is goodness-of-fit.
|| Δρ is residual electron density.

TABLE 3. Positional and isotropic thermal parameters (Å²)

		La-ClAp	Nd-ClAp	Sm-ClAp	Dy-ClAp
Ca1	z*	0.00347(9)	0.0028(1)	0.00275(7)	0.00299(9)
Ca1	B_{eq}	1.26(3)	1.13(3)	1.09(2)	1.20(3)
Ca2	x	0.00393(6)	0.00310(7)	0.00425(4)	0.00475(6)
Ca2	y	0.25895(7)	0.25786(7)	0.25877(4)	0.25894(7)
Ca2	B_{eq}	1.17(2)	1.21(2)	1.06(1)	1.15(2)
P	x	0.37530(9)	0.37501(9)	0.37556(5)	0.37565(9)
P	y	0.40780(9)	0.4074(1)	0.40809(5)	0.40844(9)
P	B_{eq}	0.97(2)	1.06(2)	0.837(8)	0.97(2)
O1	x	0.4917(2)	0.4916(2)	0.4916(1)	0.4923(2)
O1	y	0.3437(2)	0.3429(2)	0.3438(1)	0.3442(2)
O1	B_{eq}	1.37(4)	1.51(4)	1.30(2)	1.40(4)
O2	x	0.4659(2)	0.4659(2)	0.4663(1)	0.4660(2)
O2	y	0.5926(2)	0.5933(2)	0.5928(1)	0.5930(2)
O2	B_{eq}	1.41(4)	1.52(4)	1.31(2)	1.39(4)
O3	x	0.2673(2)	0.2667(2)	0.2674(1)	0.2673(2)
O3	y	0.3536(2)	0.3529(2)	0.3539(1)	0.3539(2)
O3	z	0.0677(2)	0.0678(2)	0.0676(1)	0.0675(2)
O3	B_{eq}	1.80(3)	1.97(3)	1.74(2)	1.76(3)
Cl	z	0.4448(2)	0.4480(3)	0.4497(2)	0.4495(3)
Cl	B_{eq}	1.73(6)	2.23(7)	1.75(4)	1.90(7)

Note: $B_{eq} = 4/3\ \Sigma_i\Sigma_j\ \beta_{ij}\ a_i.a_j$.
* Atomic coordinates defined by symmetry: Ca1 – x = 2/3, y = 1/3; Ca2, P, O1, O2 – z = 1/4; Cl – x = 0, y = 0.

TABLE 4. Selected bond distances (Å) and angles (°)

	La-ClAp	Nd-ClAp	Sm-ClAp	Dy-ClAp
Ca1-O1 ×3	2.4116(7)	2.4125(7)	2.4150(5)	2.4107(6)
Ca1-O2* ×3	2.451(1)	2.444(1)	2.4482(6)	2.446(1)
Ca1-O3† ×3	2.800(2)	2.804(2)	2.797(1)	2.796(1)
mean	2.554	2.553	2.553	2.551
Ca2-O1†	2.967(1)	2.956(1)	2.971(1)	2.980(1)
Ca2-O2‡	2.3042(6)	2.3121(6)	2.3025(4)	2.3034(6)
Ca2-O3 ×2	2.5487(8)	2.5493(8)	2.5462(5)	2.5415(7)
Ca2-O3§ ×2	2.338(1)	2.336(1)	2.3377(8)	2.338(1)
mean	2.507	2.506	2.507	2.507
Ca2-Cl	2.8090(9)	2.813(1)	2.8212(6)	2.820(1)
P-O1	1.530(2)	1.534(2)	1.528(1)	1.532(2)
P-O2	1.545(2)	1.553(2)	1.543(1)	1.543(2)
P-O3 ×2	1.529(1)	1.531(1)	1.5298(7)	1.531(1)
mean	1.533	1.537	1.533	1.534
O1-P-O2	111.2(1)	111.3(1)	111.18(6)	111.2(1)
O1-P-O3|| ×2	111.98(6)	111.95(6)	111.98(4)	111.98(6)
O2-P-O3 ×2	106.88(7)	106.92(7)	106.91(4)	106.95(7)
O3-P-O3||	107.7(1)	107.5(1)	107.57(7)	107.5(1)

* *–x,–y,–z.* § *x–y,x,–z.*
† *–y,x–y,z.* || *x,y,*1/2*–z.*
‡ *y–x,–x,z.*

TABLE 6. Positional and isotropic thermal parameters (Å²) for the $P2_1/b$ structures of La-ClAp and Dy-OHAp

	La-ClAp				Dy-OHAp*			
	x	y	z	B	x	y	z	B
Ca1	0.3227(2)	0.58037(8)	0.0037(2)	0.42(3)	0.3417(1)	0.58739(6)	0.0022(1)	0.70(2)
Ca1p	0.3449(2)	0.5865(1)	0.4968(2)	1.68(5)	0.3251(1)	0.58132(7)	0.4996(1)	0.80(2)
Ca2a	0.25884(5)	0.25185(3)	0.2484(4)	1.11(1)	0.24420(4)	0.24583(2)	0.2506(3)	0.694(5)
Ca2b	0.00426(5)	0.62268(3)	0.7481(4)	1.23(1)	0.99184(4)	0.62310(2)	0.7512(3)	0.693(5)
Ca2c	0.25546(5)	0.37953(3)	0.7501(4)	1.159(9)	0.25488(4)	0.37524(2)	0.7468(3)	0.675(6)
Pa	0.40750(7)	0.43754(4)	0.2555(5)	0.94(1)	0.40018(5)	0.43273(3)	0.2463(4)	0.515(7)
Pb	0.62463(7)	0.26654(3)	0.2531(6)	0.97(1)	0.62922(6)	0.26243(3)	0.2432(3)	0.529(9)
Pc	0.03239(7)	0.45376(4)	0.7535(5)	0.98(1)	0.02934(6)	0.44923(3)	0.7498(5)	0.595(6)
O1a	0.3436(2)	0.49575(8)	0.248(1)	1.37(3)	0.3309(2)	0.49239(8)	0.2592(7)	0.97(3)
O1b	0.4920(2)	0.32379(8)	0.756(1)	1.33(3)	0.4836(2)	0.32969(8)	0.7449(7)	1.02(2)
O1c	0.1481(2)	0.57837(8)	0.257(1)	1.40(4)	0.1579(2)	0.58710(8)	0.2571(9)	0.99(3)
O2a	0.5921(2)	0.48276(8)	0.2354(8)	1.17(4)	0.5853(2)	0.48025(8)	0.2618(5)	1.07(3)
O2b	0.5341(2)	0.31366(8)	0.241(1)	1.18(4)	0.5350(2)	0.31067(8)	0.2621(5)	0.99(3)
O2c	0.1268(2)	0.54621(8)	0.7332(7)	1.15(4)	0.1186(2)	0.54413(8)	0.7704(4)	1.00(3)
O3a	0.3363(3)	0.3796(2)	0.0796(5)	1.25(7)	0.3604(3)	0.3811(2)	0.0684(4)	0.56(4)
O3b	0.7399(5)	0.2901(2)	0.0755(5)	1.36(9)	0.7376(3)	0.2933(2)	0.0640(4)	0.66(4)
O3c	0.0792(4)	0.4180(2)	0.5784(5)	1.36(8)	0.0922(2)	0.4338(1)	0.5503(3)	0.85(3)
O3ap	0.3696(4)	0.3876(2)	0.4442(4)	1.06(7)	0.3359(4)	0.3742(2)	0.4199(4)	1.24(6)
O3bp	0.7260(4)	0.2968(2)	0.4407(5)	0.98(9)	0.7509(4)	0.2870(2)	0.4277(4)	1.08(5)
O3cp	0.0925(4)	0.4350(2)	0.9429(4)	0.99(7)	0.0730(2)	0.4097(1)	0.9139(2)	0.85(3)
Cl,OH	0.0017(1)	0.24930(6)	0.4451(1)	1.58(2)	0.9997(2)	0.2452(1)	0.1963(2)	1.01(3)
H					0.004(5)	0.251(2)	0.074(4)	B(OH)

* Unit-cell parameters for Dy-OHAp are: a = 9.4179(8), b = 18.8358(15), c = 6.8793(4) Å, γ = 120°.

ture of which was investigated in Fleet et al. (2000); there were 8303 independent reflections, with 6186 having $I < 3\sigma_I$; R = 0.032, R_w = 0.038, and s = 0.851.

RESULTS AND DISCUSSION

Chlorapatite compositions and REE uptake

The recovered experimental products represented 11 to 28 wt% of the starting material, and consisted of powdered Ca phosphates and a matte of fine-grained REE silicates, with scattered crystals of ClAp up to 1 mm in diameter and rare small crystals of REE silicates [e.g., $La_3(SiO_4)_2Cl$ and $Dy_2Si_2O_7$]. The REE silicate matte was a late-stage or quench product, as was the Ca phosphate powder. Starting compositions were completely melted at 900 °C, and were adjusted to minimize the proportion of equilibrium crystallization of ClAp. The REE-doped ClAp crystals were stoichiometric to within the precision of measurement by EPMA; the ratio of total cations in Ca and P positions being 1.665, 1.683, 1.660, and 1.675, for La-, Nd-, Sm-, and Dy-ClAp, respectively (Table 1), and close to the ideal value of 1.667, and Cl contents varied from 1.99 to 2.00 anions pfu. Therefore, little error was introduced in assuming ideal stoichiometry for the X-ray structure refinements. Furthermore, the hexagonal ($P6_3/m$) unit-cell volumes range from 545.44 to 546.16 Å³, which are consistent with the largest unit-cell volumes reported for crystals of ClAp grown hydrothermally (545.04 Å³; Baumer et al. 1995) and by flux growth (544.33 Å³; Bauer and Klee 1993), when allowance is made for the substitution of REE and Na for Ca (see below).

The REE contents of the present ClAp crystals were rather low (0.10 to 0.18 cations pfu) compared with the REE-doped OHAp (0.21 to 0.32 cations pfu) and FAp (0.52 to 0.82 cations pfu; Table 7) used in the single-crystal X-ray structure studies of Fleet et al. (2000) and Fleet and Pan (1995). Also, these small contents of REE in ClAp that crystallized from H_2O-bearing phosphate-chloride melts were charge compensated entirely by parallel substitution of Na for Ca, according to:

$$REE^{3+} + Na^{1+} = 2Ca^{2+};\ Ca_{10-2y}Na_yREE_y(PO_4)_6A_2 \quad (1)$$

In marked contrast, the substitution of REE for Ca in OHAp that crystallized from H_2O-bearing Na-rich phosphate melts (Fleet et al. 2000) was charge compensated almost exclusively by parallel substitution of Si for P, according to:

$$REE^{3+} + Si^{4+} = Ca^{2+} + P^{5+};\ Ca_{10-6x}REE_{6x}(P_{1-x}Si_xO_4)_6A_2 \quad (2)$$

In contrast, charge compensation for the substitution of REE for Ca in FAp that crystallized from H_2O-bearing, phosphate-fluoride melts (Fleet and Pan 1995, 1997a) was effected by parallel substitution of both Si and Na for P and Ca, respectively. Reactions 1 and 2 are the dominant substitution mechanisms for REE-bearing apatite in alkaline igneous rocks (Rønsbo 1989). The strong dependence of substitution mechanism on volatile anion component in experiments with H_2O-bearing phosphate melts appears quite unrelated to melt composition, because the ratio Na/Si in the bulk composition decreased in the sequence REE-OHAp > REE-FAp >> REE-ClAp.

The apatite crystal/melt partition coefficients (D) for REE are 0.073, 0.128, 0.122, and 0.101, for La-, Nd-, Sm-, and Dy-ClAp, respectively (Table 7), with uptake peaking at Nd, as in synthetic FAp and OHAp (Fleet and Pan 1995; Fleet et al. 2000). These D values were anomalously low compared with earlier data for REE-FAp and REE-OHAp (Fig. 1), but not inconsistent with D values inferred for apatite in Apollo 14 rocks (Jolliff et al. 1993; Fig. 1 of Fleet and Pan 1997b). Partition coefficients were > 1 for synthetic FAp and OHAp, with precise values dependent on REE content; the maximum D values observed in Fleet and Pan (1997b) were about 8–10 for minor amounts of light REE in FAp crystallized from H_2O-bearing, phosphate-fluoride melts. We note that the data for apatites synthesized

for X-ray structure studies are minimum D values because melt compositions were not corrected for liquidus crystallization, as in Fleet and Pan (1997b) and therefore liquid compositions are overestimated. However, liquidus phases were generally present in small amounts and the error here is small relative to the large difference in uptake between ClAp and OHAp and FAp. Apatite/whole rock distribution coefficients for (F,Cl)Ap solid solution in phosphate-rich Apollo 14 rocks (Jolliff et al. 1993) peaked at Sm and ranged from 0.21 to 0.86, with an average value of 0.42. The REE and Cl contents of these apatites were highly variable from sample to sample, and there was a weak inverse correlation between REE content and Cl content (Table 3 of Jolliff et al. 1993). The scatter in these data is diminished significantly by noting that the sample with highest Cl content and 890 ppm Sm has an anomalously high content of Si.

Fleet and Pan (1997b) suggested that the chemistry of REE in the melt (or fluid), as well as other physicochemical parameters, may exert greater control on REE uptake than apatite crystal chemistry, and speculated that the absence of H_2O in lunar basaltic magma was the most significant factor limiting the uptake of REE by the Apollo 14 apatites. A simple melt complexation explanation now appears untenable in light of the uptake data for end-member REE-OHAp (Fleet et al. 2000) and REE-ClAp. Hydroxylapatite is not a more favorable host for REE than FAp, and ClAp is also impoverished in REE when crystallized from H_2O-bearing phosphate-chloride melts. Moreover, we have seen that, although the substitution mechanism (Eq. 1 and 2) for the incorporation of REE in apatite correlates strongly with volatile anion component, it is apparently independent of the actual concentration of Na and Si in the bulk (or melt). However, the case for a crystal-chemical control on REE uptake by apatite is not straightforward, and the influence of melt (or fluid) composition cannot be excluded, because a significant Cl content in apatite alone does not apparently inhibit the incorporation of REE. Whereas the uptake of REE by ClAp and (F,Cl)Ap is relatively low, the apatite/melt partition coefficients derived in Fleet and Pan (1997b) for (Cl,OH)Ap from spinel lherzolites from Yemen (Chazot et al. 1996) were generally >1 and similar to those for FAp grown from H_2O-bearing phosphate-fluoride melts.

TABLE 7. REE site occupancies and site-occupancy ratio

		La-ClAp	Nd-ClAp	Sm-ClAp	Dy-ClAp
Ca1 site occupancy-	Ca	0.963	0.983	0.927	0.933
	Na	0.025	0.0	0.041	0.036
	REE	0.0126	0.0172	0.0322	0.0306
Ca2 site occupancy-	Ca	0.991	0.952	0.993	0.997
	Na	0.0	0.029	0.0	0.0
	REE	0.0089(6)	0.0191(5)	0.0069(3)	0.0026(5)
REE-Ca2/REE-Ca1		0.71(8)	1.11(7)	0.21(1)	0.09(2)
Total REE (pfu*)		0.104	0.184	0.170	0.138
ΔV† (Å³)		+1.12	+1.02	+0.58	+0.40
D_{REE}‡		0.073	0.128	0.122	0.101
		La-OHAp	Nd-OHAp	Sm-OHAp	Dy-OHAp
REE-Ca2/REE-Ca1		10.5	2.0	1.63	3.3
Total REE (pfu)		0.286	0.316	0.270	0.212
ΔV† (Å³)		+2.75	+0.41	+0.27	–0.17
		La-FAp	Nd-FAp	Gd-FAp	Dy-FAp
REE-Ca2/REE-Ca1		4.01	2.86	2.00	1.46
Total REE (pfu)		0.650	0.820	0.612	0.518
ΔV† (Å³)		+6.03	+3.59	+1.22	+0.70
		La,Gd-FAp	Ce,Dy-FAp	Pr,Er-FAp	Eu,Lu-FAp
REE-Ca2/REE-Ca1		2.30	2.29	2.00	1.71
Total REE (pfu)		0.606	0.504	0.474	0.404
ΔV† (Å³)		+3.47	+2.82	+1.94	+0.92

* $Ca_{10}(PO_4)_6Cl_2$.
† Deviation from unit-cell volume of end-member ClAp/OHAp/FAp (Baumer et al. 1995/Elliott 1998/Sudarsanan 1972).
‡ D(REE; apatite/melt).

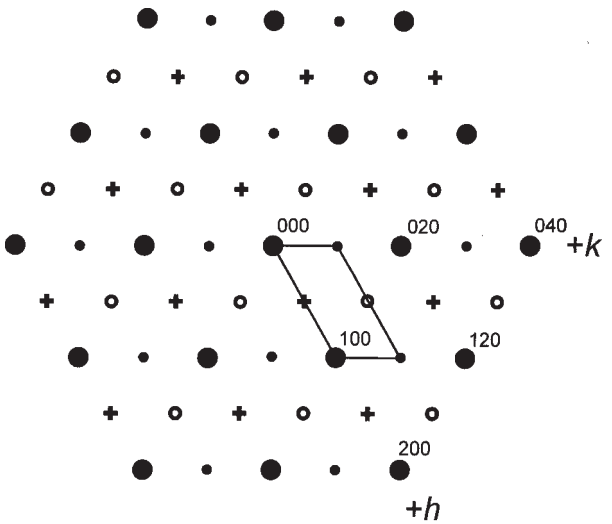

FIGURE 3. Sketch of 00*l* diffraction pattern of twinned monoclinic ClAp: large full circles are overlapped reflection triplets equivalent in $P6_3/m$; small full circles, small open circles and pluses are $P2_1/b$ superstructure reflections.

Monoclinic ($P2_1/b$) structure

The crystals of REE-doped ClAp were monoclinic with $b \approx 2a$ and $\gamma \approx 120°$ (space group $P2_1/b$; Table 2), and mimetic twinned. The twinned diffraction pattern (Fig. 3) has hexagonal symmetry and corresponds to a = 2a', c = c' (where a' and c' are parameters of the $P6_3/m$ subcell). Twinning was also encountered in the double-REE-substituted FAp crystals of Fleet and Pan (1997a), in which the twin individuals were related by 180% rotation about the *c* axis so that reflection pairs [*hkl*; *h*,–(*h*+*k*),*l*], which are non-equivalent in $P6_3/m$, had equal intensity. This was evidently growth twinning.

Conversely, for the present REE-doped ClAp, the reflection pairs [*hkl*; *h*,–(*h*+*k*),*l*] are non-equivalent, showing that the crystals are untwinned and have the hexagonal $P6_3/m$ structure under the conditions of synthesis. Superstructure reflections that are characteristic of the monoclinic cell were not overlapped by the twin operation (Fig. 3), but reflection triplets equivalent in $P6_3/m$ were. Thus, the twinned diffraction pattern of the present REE-doped ClAp crystals is consistent with displacive $P6_3/m \rightarrow P2_1/b$ transformation twinning on quenching.

The intensity of the monoclinic $P2_1/b$ superstructure reflections of La-ClAp (which has the lowest REE content) was slightly greater than that calculated for the ClAp crystal investigated by Mackie et al. (1972): e.g., the powder-XRD intensity of the superstructure reflection 212 was 4.8% for the present La-ClAp and 3.5% for the ClAp of Mackie et al. (1972). In

making this comparison: (1) equivalent observed powder-XRD intensities were obtained for La-ClAp by weighting the single-crystal intensities with reflection multiplicity; (2) 212 was selected for reference because it is a strong superstructure reflection; (3) the program POWD2 (Penn State University) was used to calculate powder intensities for the ClAp structure of Mackie et al. (1972); and (4) and intensities are relative to 100% for 300. However, the intensity of the superstructure reflections varied markedly with the extent of substitution of REE for Ca. This result is demonstrated in Figure 4, where we compared the average equivalent P-XRD intensities for the nine strongest observed superstructure reflections out to $d_{hkl} \approx 2.385$ Å (012, $1\bar{1}2$, $1\bar{3}2$, 112, $2\bar{1}2$, 132, $1\bar{5}2$, $2\bar{5}2$, 212) with the contents of REE and (REE + Na) cations pfu for La-, Nd-, Sm-, and Dy-ClAp. Clearly, substitution of even small amounts of Ca by REE in ClAp degrades the monoclinic $P2_1/b$ superstructure. Degradation of the superstructure, which largely represents ordering of Cl within the *c*-axis columns through substitution of Cl by vacancies, F, or OH, is well known (Prener 1967, 1971; Ruszala and Kostiner 1975; Elliott 1994). This is the first report of the effect of substituents in Ca positions on ordering of Cl atoms in stoichiometric end-member ClAp (cf., Elliott 1994). We suggest that REE cations interfere with ordering of Cl atoms during the $P6_3/m \rightarrow P2_1/b$ transition through either the local strain field resulting from their spatial accommodation or a charge-balance constraint.

The reflection intensities for the $P2_1/b$ structure of La-ClAp were detwinned using the procedure of Fleet and Burns (1990) and Fleet and Pan (1997a), and the structure was refined using the Ca1 and Ca2 site occupancies from the $P6_3/m$ refinement. The positional and isotropic thermal parameters given in Table 6 are in reasonable agreement with the data of Mackie et al. (1972) who investigated an untwinned crystal of end-member ClAp. However, because of the limited number of superstructure reflections with $I > 3\sigma_I$, the refinement with anisotropic thermal parameters was not successful and it was not meaningful to extend the present refinement to the occupancies of the five non-equivalent Ca positions. In any case, it is likely that the Ca site populations were essentially unaffected by the displacive $P6_3/m \rightarrow P2_1/b$ transition because this would occur at or below about 350 °C (Bauer and Klee 1993). In summary, our refinement of the $P2_1/b$ superstructure of La-ClAp confirms the structure of Mackie et al. (1972); the superstructure reflection intensity largely represents ordering of Cl atoms displaced along [001], and the contributions from displacement of other atoms in the structure (cf., Table 6) are relatively insignificant.

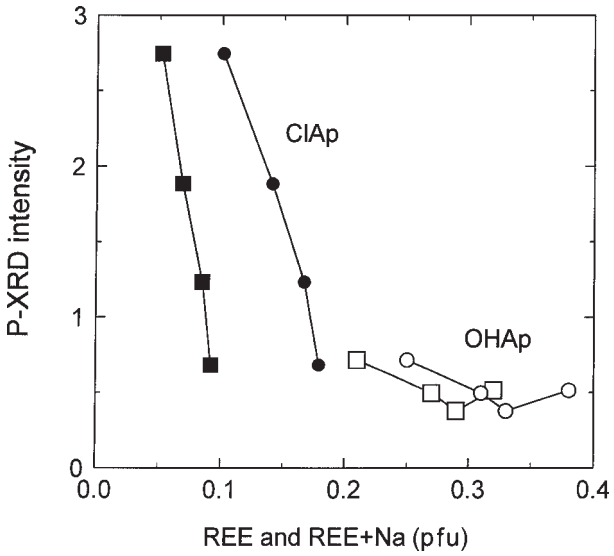

FIGURE 4. Variation of equivalent powder-XRD intensity of monoclinic $P2_1/b$ superstructure reflections with REE and (REE + Na) contents for REE-ClAp (full squares and circles, respectively) and REE-OHAp (open squares and circles); intensities are relative to 100% for the 300 reflection and are averages of nine observed single crystal reflections (012, $1\bar{1}2$, $1\bar{3}2$, 112, $2\bar{1}2$, 132, $1\bar{5}2$, $2\bar{5}2$, 212) weighted by reflection multiplicity.

We have reprocessed the CCD diffractometer data for the OHAp crystals of Fleet et al. (2000) to further investigate the effect of substitution of REE for Ca on the $P2_1/b$ superstructure reflections of OHAp. These crystals had higher contents of REE (0.21 to 0.32 cations pfu) than the present ClAp crystals and the superstructure reflections were correspondingly much weaker (Fig. 4). For Dy-OHAp (which had the lowest REE content), the equivalent observed P-XRD intensity of the reference reflection 212 was 1.4% compared with 2.1% calculated for the OHAp structure of Ikoma et al. (1999). However, the plot of average equivalent P-XRD intensity vs. the contents of REE and (REE + Na) cations for OHAp is not continuous with that for REE-ClAp, showing that the response of the $P2_1/b$ superstructure to substitution of Ca by REE is not quantitatively transferrable from ClAp to OHAp. The reflection intensities for the $P2_1/b$ structure of Dy-OHAp were detwinned and the monoclinic $P2_1/b$ structure was refined similarly to that of La-ClAp. The positional parameters are similar to the results of Elliott et al. (1973) who investigated a twinned single crystal of OHAp and, despite the very limited number of superstructure reflections with $I > 3\sigma_I$, the refinement is superior to the recent Rietveld powder structure refinement of OHAp (Ikoma et al. 1999).

Accommodation of REE in $P6_3/m$ structure

All REE site occupancies in ClAp were obtained from refinements of the $P6_3/m$ apatite-type structure. In the ideal structure, which is found only for fluorapatite, the volatile anion is centered in a three-membered ring of Ca2 atoms, at $z = 1/4, 3/4$. An important feature of the structure is that volatile anions differing greatly in size can be accommodated by displacement out of the plane of the ideal $XCa2_3$ (X = F, OH, Cl) cluster along [001]. The coordination of the X anion is then trigonal pyramidal rather than trigonal. Thus, the Ca2-X distances in FAp, OHAp, and ClAp are 2.31, 2.39, and 2.81 Å, respectively, which are broadly similar to Ca-X distances of 2.37 Å in fluorite, 2.37 Å in $Ca(OH)_2$, and 2.74 Å in $CaCl_2$, respectively. In contrast, the Ca2-X' distances for trigonal coordination are 2.31, 2.36, and 2.48 Å, respectively. Although the Ca2-X and Ca2-X' distances in FAp are nominally the same, Fleet et al. (2000)

noted that in both end-member and REE-doped FAp (Mackie and Young 1973; Sudarsanan et al. 1972; Fleet and Pan 1995, 1997a), the thermal parameter of F parallel to *c* is exaggerated ($U_{33} \approx 10 \times U_{11}$) beyond that expected for thermal motion alone, indicating that the F^- anion is also displaced out of the plane of Ca2 atoms and that it is disordered.

Refinement of the present REE-substituted ClAp structures to extract REE site occupancies followed the procedures used for REE-FAp in Fleet and Pan (1995), except that the occupancy of Si on the P position was set to zero (cf., Table 1). Only the REE site occupancy of Ca2 was refined by least squares. Other Ca1 and Ca2 site occupancies were constrained to the crystal compositions using the algorithm given in Fleet and Pan (1997a) and Fleet et al. (2000). The site occupancy of Na was refined by iteration. The resulting occupancies (Table 7) were surprising in that La, Sm, and Dy favored the Ca1 position but Nd showed little site preference; the REE site occupancy ratios [(REE-Ca2)/(REE-Ca1)] are being 0.71, 1.11, 0.21, and 0.09 for La-, Nd-, Sm-, and Dy-ClAp, respectively. Also, whereas Na was restricted to the Ca1 position in La-, Sm-, and Dy-ClAp, as in La- and Dy-FAp (Fleet and Pan 1995) and as assumed for natural REE-(F,OH)Ap in Hughes et al. (1991) and double-REE-FAp in Fleet and Pan (1997a), it favored the Ca2 position in Nd-ClAp. Moreover, when Na was assigned wholly to the Ca1 position in Nd-ClAp, the REE site occupancy ratio changed to 0.55 and resulted in a monotonic decrease in this ratio through the 4*f* transition metal series analogous to that found for FAp (Fleet and Pan 1995, 1997a) and La-OHAp to Sm-OHAp (Fleet et al. 2000). However, Ca-O bond distances and sizes of Ca polyhedra in the apatite structure are extremely sensitive to site populations and, as detailed below, independently confirm the anomalous behavior of Nd. Also, Na marginally favors (52%) the Ca2 position in Nd-FAp (Fleet and Pan 1995).

From systematic analysis of site occupancies and structural change in REE-substituted FAp, OHAp, and ClAp, it is now apparent that the crystal chemical factors that determine site preference and uptake of REE in apatite are complex, and include substitution mechanism, spatial accommodation, and a possible crystal-field-stabilization component for Nd. We have already noted that REE uptake correlates strongly with volatile anion component (X) and substitution mechanism, which are in turn closely correlated and perhaps interdependent. The REE site occupancy ratio also broadly correlates with substitution mechanism (Table 7); e.g., for La-doped apatites, this ratio is 11 in OHAp (with charge compensated by Si), 4 in FAp (with charge compensated by both Na and Si), and 0.71 in ClAp (with charge compensated by Na). These observations support the conclusion of Mackie and Young (1973), who found that minor amounts of Nd substitute for Ca in both Ca1 and Ca2 positions in NdF_3-doped Fap, but only in Ca2 in Nd_2O_3-doped FAp. However, whereas REE^{3+} in Ca2 should compensate the substitution of O^{2-} for F^- more readily than REE^{3+} in Ca1, simple explanations for the charge compensation of REE in Ca2 by Si and of REE in Ca1 by Na are much less obvious (Fleet et al. 2000).

In (F,OH)Ap solid solution, the REE site-occupancy ratio correlated with equalization of bond valence [Hughes et al. 1991; Fleet and Pan 1995, 1997a; Fleet et al. (2000); the last study noted that the FAp crystals investigated in their previous studies were not of end-member composition, but varied from 81 to 100% FAp, 19 to 0% OHAp]. It appeared from these studies that the substitution of REE for Ca in Ca2 compensated underbonding of the X anion in the end-member structures. In REE-OHAp, the correlation of site occupancy with bond valence was complicated by the effects of spatial accommodation (Fleet et al. 2000). Bond valences were not calculated for the present REE-ClAp structures due to the lack of appropriate coefficients for bonds to Cl.

As summarized in Fleet et al. (2000), substitution of the anion component resulted in a progressive increase in *a* and unit-cell volume and decrease in *c* in the sequence FAp→ OHAp→ ClAp. The volume of the Ca2 polyhedron increased almost linearly by about 8% from FAp to ClAp, but that of the Ca1 polyhedron increased by only 0.7% and the variation with composition is complex (Fig. 5). This analysis of the affect of the anion component on the apatite structure recognized that the natural FAp, OHAp, and ClAp crystals investigated in Hughes et al. (1989) were not of end-member composition. Incorporation of REE into apatite (La → Dy in FAp and ClAp, and La → Sm in OHAp) resulted in a differential increase in the size of both Ca polyhedra (Fig. 5); considering that the REE occupancies of Ca1 in FAp and OHAp are generally appreciably lower than those of Ca2, the response of the Ca1 polyhedron is somewhat greater than that of Ca2. Individual trend lines for the substitution of Ca by REE in a given Ca polyhedron are almost parallel and extrapolate back to the corresponding REE-free end-member (Fig. 5). Note that the volume of the Ca1 polyhedron of Nd-ClAp is relatively low and indicates that occupancy of Nd in Ca1 is significantly lower than that of La and Sm, but consistent with the present unconstrained least-squares refinement (Table 7).

Progressive change in individual Ca-O bond distances and O-Ca-O bond angles with substitution of REE for Ca in apatite is not continuous but tends to hinge at Nd (see also Fleet and Pan 1997a). In Figure 6, the change in the Ca2-O1 distance in REE-doped FAp, OHAp, and ClAp is shown relative to the smallest REE^{3+} cation investigated (Dy) and highlights an anomalous contraction at Nd. Moreover, incorporation of Nd results in an overall decrease in size of the Ca2 polyhedron (Fig. 7a), even though this element is present in greater abundance than neighboring REE cations (La and Sm,Gd). Clearly, the anomalies at Nd are not consistent with the incorporation of spherical, hard-shell cations of progressively increasing (or decreasing) radius. We suggest that Nd imposes a local Jahn-Teller distortion on the Ca2 position. We emphasize that anomalous contraction of the Ca2-O1 distance at Nd is independent of the considerable structural distortion resulting from occupation of the volatile anion position (X) by F, OH, and Cl. Anomalies in plots of polyhedral volume and bond distances for Ca1 (e.g., Fig. 7b) largely reflect differential occupancy of Ca1 by REE (e.g., the relatively low contents of Nd in Ca1 of ClAp and high contents of Nd in FAp) and preferential accommodation of Sm in OHAp (Fleet et al. 2000). The 4*f* crystal-field effect should be stronger for the Ca2 position because of its asymmetric crystal field (formed by the hemisphere of six

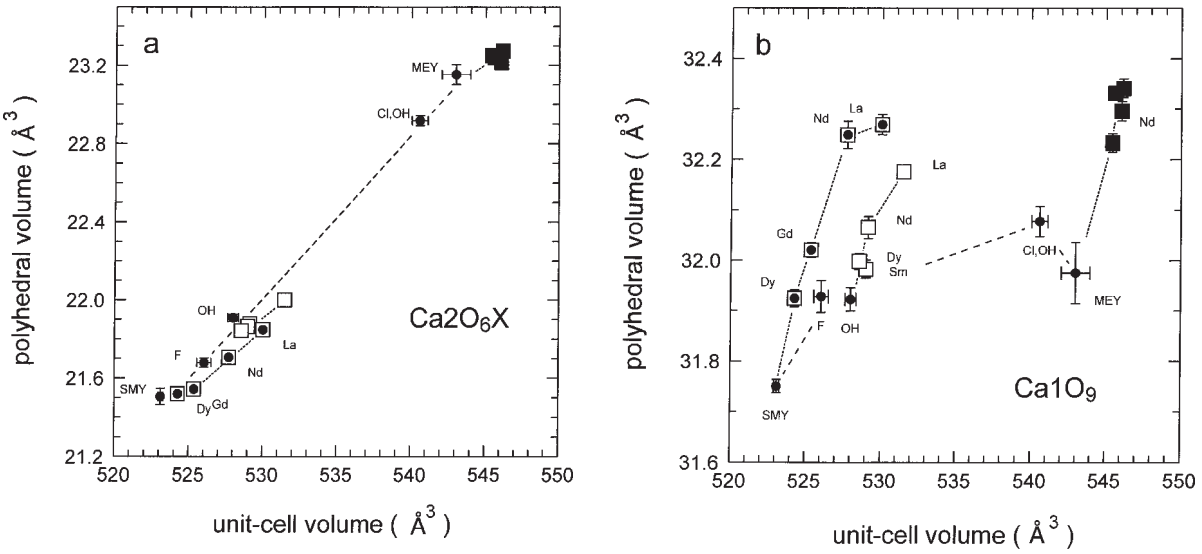

FIGURE 5. Variation in volume of $Ca2O_6X$ polyhedron (**a**) and $Ca1O_9$ polyhedron (**b**) with unit-cell volume for REE-ClAp (present study; full squares), REE-FAp (Fleet and Pan 1995; open squares with dot), REE-OHAp (Fleet et al. 2000; open squares), and synthetic (Sudarsanan et al. 1972; SMY; Mackie et al. 1972; MEY) and natural (Hughes et al. 1989) FAp, OHAp and (Cl,OH)Ap (full circles): trend lines have been fitted visually; polyhedral volumes with errors were calculated with VOLCAL (Hazen and Finger 1982); error bars are ±1σ and are partly obscured by symbol size for REE-substituted apatites.

oxygen atoms capped by the volatile anion component, X; Fig. 2), and more pronounced for Pr and Nd than adjacent REE and heavy REE, and absent for La, Gd, and Lu (e.g., Morss 1976). This interpretation is consistent with Hughes et al. (1993), who suggested that the strong preference shown by Fe^{2+} for the Ca2 position of an Fe-bearing apatite with monoclinic, $P2_1/m$, symmetry resulted from a contribution by (3*d*) crystal-field stabilization energy.

Fleet et al. (2000) showed that minimization of volume strain is an important factor in the dominant preference of REE (and particularly of the larger light REE) for the Ca2 position in FAp and OHAp. Plots of the REE site occupancy ratio vs. change in cell volume relative to end-member structures converged toward [(REE-Ca2)/(REE-Ca1)] = 1 at $\Delta v_{\text{unit cell}} = 0$. However, minimization of volume strain does not appear to exert significant control on the dominant preference of La, Sm, and Dy for Ca1 in ClAp; the REE site occupancy ratio for these cations becomes progressively smaller with decreasing $\Delta v_{\text{unit cell}}$ (Table 7). Although it is not intuitively obvious why substitution mechanism should radically modify REE site preference in ClAp based on charge-balance considerations, the substitution of F and OH by Cl does result in differential expansion and distortion of the Ca sites. Thus, the much greater size of Ca2 in ClAp may have diminished the selectivity of this position for REE relative to that of Ca1. For Nd, this effect is partially compensated by a significant 4*f* crystal-field stabilization, which accounts for its anomalous Ca2/Ca1 site occupancy ratio (1.11).

The present REE site-occupancy results demonstrate that the peak at Nd-Gd in REE uptake curves for apatite is not exclusively related to a strong preference of REE for the Ca2 position. The uptake curve for ClAp crystallized from H_2O-bearing phosphate-chloride melts remains peaked at Nd even though REE have a dominant preference for Ca1. However, the overall form of the REE uptake curve for apatites does appear to be related to spatial accommodation of REE in the apatite structure. The simple analysis in Fleet and Pan (1997b) that was based on comparison of ideal bond distances calculated using effective ionic radii for REE^{3+} and Ca^{2+} (Shannon

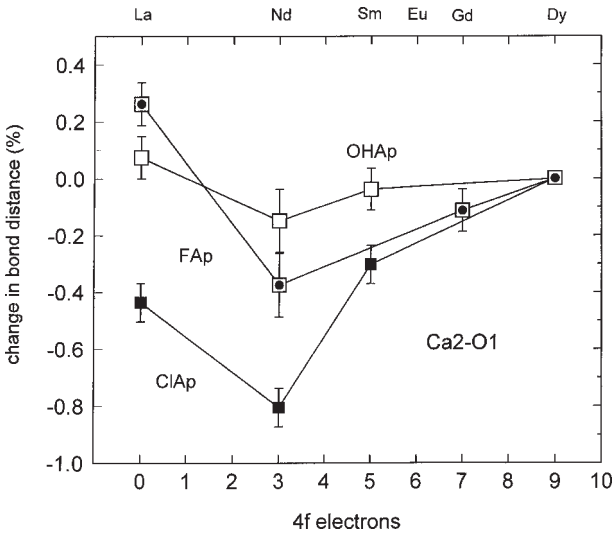

FIGURE 6. Change in Ca2-O1 bond distance of REE-substituted apatites with substitution of REE relative to Dy-Ap, showing anomalous decrease at Nd; error bars are ±1σ.

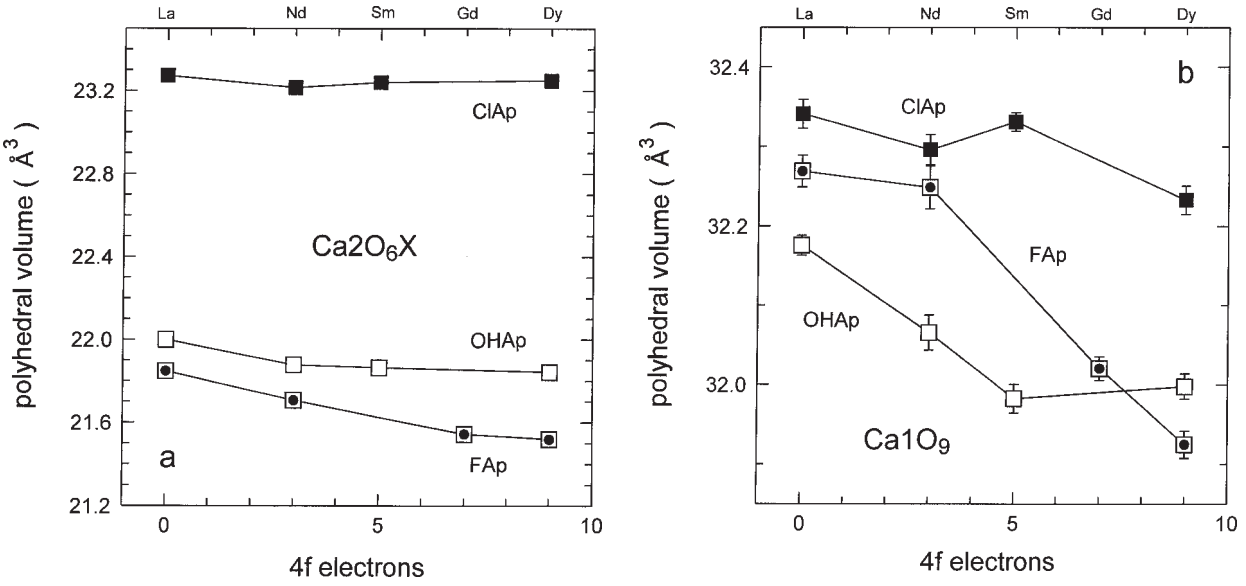

FIGURE 7. Change in volume of $Ca2O_6X$ polyhedron (**a**) and $Ca1O_9$ polyhedron (**b**) with substitution of REE into ClAp: REE contents are given in Table 7; error bars are ±1σ and are obscured by symbol size in **a**.

1976) remains valid, even though the prediction of a more light-REE-enriched pattern for ClAp is contradicted by this study. Fleet and Pan (1997b) assumed that Ca2 would remain the preferred Ca position for incorporation of REE in ClAp. The form of the theoretical uptake pattern derived using the present site occupancies (which reveal a strong preference of La, Sm, and Dy for Ca1) is not unlike the form of the observed uptake pattern (Fig. 1). Peaking of the uptake pattern at Nd in our experimental studies is attributed to a 4*f* crystal-field contribution in FAp, OHAp, and ClAp. In natural apatites, the tendency for a Jahn-Teller distortion could well be mitigated by complex REE site occupancies in the Ca2 position and by (F, OH, Cl, O) site occupancies in the volatile anion position. Of course, the wide variations in REE contents of apatites and REE uptake (e.g., Fig. 1; Fig. 1 of Fleet and Pan 1997b) must reflect the combined effects of melt (or fluid) chemistry and substitution mechanism.

ACKNOWLEDGMENTS

We thank John Hughes and an unnamed reviewer for helpful comments, Michael Jennings for assistance with collection of X-ray reflection data and the Natural Sciences and Engineering Research Council of Canada for financial support.

REFERENCES CITED

Argiolas, R. and Baumer, A. (1978) Synthèse de chlorapatite par voie hydrothermale: Étude de l'influence de la sursaturation sur l'évolution des faciès des cristaux. Canadian Mineralogist, 16, 285–290.

Bauer, M. and Klee, W.E. (1993) The monoclinic-hexagonal phase transition in chlorapatite. European Journal of Mineralogy, 5, 307–316.

Baumer, A., Gibert, R., Vernay, A.-M., and Lapraz, D. (1995) Incorporation d'ions hydroxyles dans la chlorapatite: caractérisation par spectrométrie infrarouge (réflexion diffuse). Compte Rendu Académie des Sciences Paris, 321, 579–584.

Chazot, G., Menzies, M.A., and Harte, B. (1996) Determination of partition coefficients between apatite, clinopyroxene, amphibole, and melt in natural spinel lherzolites from Yemen: Implications for wet melting of the lithospheric mantle. Geochimica et Cosmochimica Acta, 60, 423–437.

Elliott, J.C. (1994) Structure and Chemistry of the Apatites and Other Calcium Orthophosphates. Elsevier, Amsterdam.

Elliott, J.C. (1998) Recent studies of apatites and other calcium orthophosphates, In E. Brès and P. Hardouin, Eds., Les matériaux en phosphate de calcium, Aspects fondamentaux, 25, p. 25–66. Sauramps Medical, Montpellier.

Elliott, J.C., Mackie, P.E., and Young, R.A. (1973) Monoclinic hydroxyapatite. Science, 180, 1055–1057.

Fleet, M.E. and Burns, P.C. (1990) Structure and twinning of cobaltite. Canadian Mineralogist, 28, 719–723.

Fleet, M.E. and Pan, Y. (1995) Site preference of rare earth elements in fluorapatite. American Mineralogist, 80, 329–335.

———(1997a) Site preference of rare earth elements in fluorapatite: Binary (LREE+HREE)-substituted crystals. American Mineralogist, 82, 870–877.

———(1997b) Rare earth elements in apatite: Uptake from H_2O-bearing phosphate-fluoride melts and the role of volatile components. Geochimica et Cosmochimica Acta, 61, 4745–4760.

Fleet, M.E., Liu, X., and Pan, Y. (2000) Site preference of rare earth elements in hydroxyapatite [$Ca_{10}(PO_4)_6(OH)_2$]. Journal of Solid State Chemistry, 149, 391–398.

Gunawardane, R.P., Howie, R.A., and Glasser, F.P. (1982) Structure of the oxyapatite $NaY_9(SiO_4)_6O_2$. Acta Crystallographica, B38, 1564–1566.

Hazen, R.M. and Finger, L.W. (1982) Comparative Crystal Chemistry. Wiley, New York.

Hughes, J. M., Cameron, M., and Crowley, K. D. (1989) Structural variations in natural F, OH, and Cl apatites. American Mineralogist, 74, 870–876.

Hughes, J.M., Cameron, M., and Mariano, A.N. (1991) Rare-earth-element ordering and structural variations in natural rare-earth-bearing apatites. American Mineralogist, 76, 1165–1173.

Hughes, J.M., Fransolet, A.-M., and Schreyer, W. (1993) The atomic arrangement of iron-bearing apatite. Neues Jahrbuch für Mineralogie, Monatshefte, 1993, 504–510.

Hunslow, A.W. and Chao, G.Y. (1969) Monoclinic chlorapatite from Ontario. Canadian Mineralogist, 10, 252–259.

Ibers, J.A. and Hamilton, W.C., Eds. (1974) International tables for X-ray crystallography, vol. 4. Kynoch Press, Birmingham, England.

Ikoma, T., Yamazaki, A., Nakamura, S., and Akao, M. (1999) Preparartion and structure refinement of monoclinic hydroxyapatite. Journal of Solid State Chemistry, 144, 272–276.

Jarosewich, E. and Boatner, L.A. (1991) Rare earth element reference samples for electron microprobe analysis. Geostandards Newsletter, 15, 397–399.

Jolliff, B.L., Haskin, L.A., Colson, R.O., and Wadhwa, M. (1993) Partitioning in REE-saturating minerals: Theory, experiment and modelling of whitlockite,

apatite, and evolution of lunar residual magmas. Geochimica et Cosmochimica Acta, 57, 4069–4094.
Mackie, P.E. and Young, R.A. (1973) Location of Nd dopant in fluorapatite, $Ca_5(PO_4)_3F$:Nd. Journal of Applied Crystallography, 6, 26–31.
Mackie, P.E., Elliott, J.C., and Young, R.A. (1972) Monoclinic structure of synthetic $Ca_5(PO_4)_3Cl$, chlorapatite. Acta Crystallographica, B 28, 1840–1848.
Morss, L.S. (1976) Thermochemical properties of yttrium, lanthanum, and lanthanide elements and ions. Chemical Reviews, 76, 827–841.
Prener, J.S. (1967) The growth and crystallographic properties of calcium fluor- and chlorapatite crystals. Journal of the Electrochemical Society, 114, 77–83.
Prener, J.S. (1971) Nonstoichiometry in calcium chlorapatite. Journal of Solid State Chemistry, 3, 49–55.
Rønsbo, J.G. (1989) Coupled substitutions involving REEs and Na and Si in apatites in alkaline rocks from the Ilimaussaq intrusion, South Greenland, and the petrological implications. American Mineralogist, 74, 896–901.
Ruszala, F. and Kostiner, E. (1975) Preparation and characterization of single crystals in the apatite system $Ca_{10}(PO_4)_6(Cl,OH)_2$. Journal of Crystal Growth, 30, 93–95.
Shannon, R.D. (1976) Revised effective ionic radii and systematic studies of interatomic distances in halides and chalcogenides. Acta Crystallographica, A32, 751–767.
Sudarsanan, K., Mackie, P.E., and Young, R.A. (1972) Comparison of synthetic and mineral fluorapatite, $Ca_5(PO_4)_3F$, in crystallographic detail. Materials Research Bulletin, 7, 1331–1338.
Takahashi, M., Uematsu, K., Ye, Z.-G., and Sato, M. (1998) Single-crystal growth and structure determination of a new oxide apatite, $NaLa_9(GeO_4)_6O_2$. Journal of Solid State Chemistry, 139, 304–309.
Urusov, V.S. and Khudolozhkin, V.O. (1974) An energy analysis of cation ordering in apatite. Geochemistry International, 11, 1048–1053.

MANUSCRIPT RECEIVED NOVEMBER 18, 1999
MANUSCRIPT ACCEPTED MAY 9, 2000
PAPER HANDLED BY BRAD L. JOLLIFF